

## Evolution of the Most Massive Stars

André Maeder, Georges Meynet & Raphael Hirschi

*Geneva Observatory, CH-1290 Sauverny, Switzerland*

**Abstract.** We discuss the physics of the  $\Omega\Gamma$ -Limit, i.e. when the star is unbound as a result of *both* rotation and radiation pressure. We suggest that the  $\Omega\Gamma$ -Limit is what makes the Humphreys–Davidson Limit. Stellar filiations are discussed, with an emphasis on the final stages, in particular on the final masses, their angular momentum and the chemical yields with account of rotation. A possible relation between WO stars and GRB is emphasized.

### 1. Introduction

Massive stars are at the crossroads of major subjects in Astrophysics. They have a key influence on the spectral and chemical evolution of galaxies. Their contributions to the spectrum of starbursts is observed up to large redshifts. They are also the essential components of the metallicity  $Z = 0$  populations, the progenitors of WR stars, supernovae and gamma ray bursts (GRB).

### 2. The $\Omega\Gamma$ -Limit: physics of the interaction of mass loss and rotation

The physics and evolution of massive stars is dominated by mass loss and by rotational mixing. At the origin of these two effects, we find the large ratio  $T/\rho$  of temperature to density in massive stars. This enhances the ratio of radiation to gas pressure, which goes like  $T^3/\rho$  and favours stellar winds. A high  $T/\rho$  enhances rotational mixing, since mixing by shear turbulence scales as the thermal diffusivity  $K = 4acT^3/3c_p \kappa \rho^2$ . Also, the velocity of meridional circulation scales as the ratio  $L/M$  of the luminosity to mass.

Let us recall that there are 3 main effects of rotation. 1) Structural effects due to the centrifugal force: these are small in the interior, but may produce a large distorsion at the surface. 2) Rotational mixing: this produces internal transports of chemical elements and angular momentum. Mixing by shears is most efficient for the transport of chemical elements (Zahn 1992; Meynet & Maeder 2001), while meridional circulation dominates the transport of angular momentum. 3) Enhancement of mass loss by rotation: an important case is the  $\Omega\Gamma$ -Limit, where the star reaches break-up as a result of both high radiation pressure and rotation. The von Zeipel theorem states that the local radiative flux  $F$  of a rotating star is proportional to the effective gravity  $g_{\text{eff}}$ . Thus, there is a much larger flux and a higher  $T_{\text{eff}}$  at the pole than at the equator (Meynet & Maeder 1997). This latitudinal dependence of  $T_{\text{eff}}$  leads to asymmetric mass loss and also to enhanced average mass loss rates.

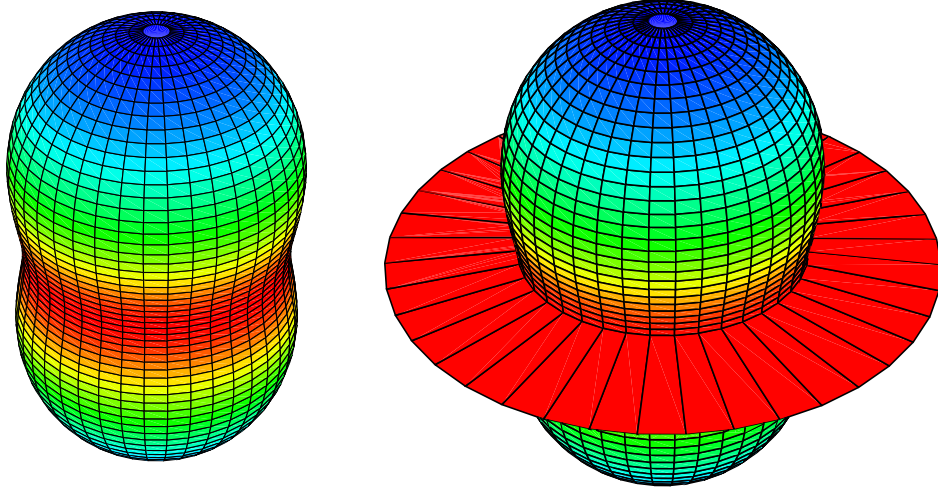


Figure 1. Left: Iso-mass loss distribution for a  $120 M_{\odot}$  star with  $\log \frac{L}{L_{\odot}} = 6.0$  and  $T_{\text{eff}} = 30000$  K rotating at a fraction 0.80 of break-up velocity. Right: The same with  $T_{\text{eff}} = 25000$  K.

On a rotating star, one must consider the flux  $F(\vartheta)$  at a given colatitude  $\vartheta$  as given by von Zeipel's theorem,  $F(\vartheta) = -\frac{L(P)}{4\pi GM_*} g_{\text{eff}} [1 + \zeta(\vartheta)]$ . The term  $\zeta(\vartheta)$  is in general negligible. The Eddington factor is a local quantity  $\Gamma_{\Omega}(\vartheta)$  depending on  $\vartheta$  and rotation. We define it as the ratio of the local flux  $F(\vartheta)$  given by the von Zeipel theorem to the maximum possible local flux, which is  $F_{\text{lim}}(\vartheta) = -\frac{c}{\kappa(\vartheta)} g_{\text{eff}}(\vartheta)$ . Thus, one has

$$\Gamma_{\Omega}(\vartheta) = \frac{F(\vartheta)}{F_{\text{lim}}(\vartheta)} = \frac{\kappa(\vartheta) L(P)}{4\pi cGM \left(1 - \frac{\Omega^2}{2\pi G\rho_m}\right)}, \quad (1)$$

where the opacity  $\kappa(\vartheta)$  depends on the colatitude  $\vartheta$ , since  $T_{\text{eff}}$  itself depends on  $\vartheta$ . For electron scattering,  $\kappa$  is constant and  $\Gamma_{\Omega}(\vartheta)$  is the same at all latitudes, i.e.  $\Gamma_{\Omega} = \Gamma / \left(1 - \frac{\Omega^2}{2\pi G\rho_m}\right)$ , where  $\Gamma$  is the usual expression. Eq. (1) shows that the maximum luminosity of a rotating star is reduced by rotation. We see that the dependences of  $F(\vartheta)$  and of  $F_{\text{lim}}(\vartheta)$  with respect to  $g_{\text{eff}}$  have cancelled each other in the expression of  $\Gamma_{\Omega}(\vartheta)$ . Thus, if the limit  $\Gamma_{\Omega}(\vartheta) = 1$  happens to be met at the equator, it is not because  $g_{\text{eff}}$  is the lowest there, but because the opacity is the highest! The theory of radiative winds applied to a rotating star leads to an expression of the mass flux as a function of colatitude (Maeder 1999). Figs. 1 left and right (Maeder & Desjacques 2000) illustrate the distribution of the mass loss rates around a massive star of  $120 M_{\odot}$  for two different  $T_{\text{eff}}$ . For a star hot enough to have electron scattering opacity from pole to equator, the iso-mass

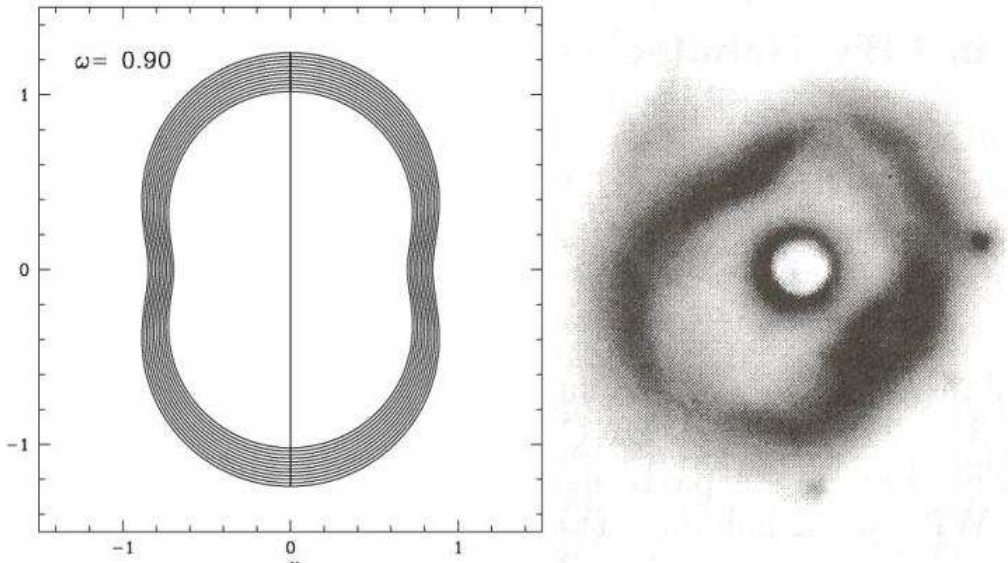


Figure 2. Left: simulation of a short shell ejection by a massive star with anisotropic mass loss as in Fig. 1 left. Right: the nebulae around AG Carinae (Nota & Clampin 1997).

loss curve has a peanut-like shape (Fig. 1 left). This results from the fact that the pole is hotter (“ $g_{\text{eff}}$ -effect”). For a rotating star with a lower  $T_{\text{eff}}$  (Fig. 1 right), a bistability limit i.e. a steep increase of the opacity (Lamers et al. 1995) may occur somewhere between the pole and the equator. This “opacity-effect” produces an equatorial enhancement of the mass loss (Fig. 1 right). In Fig. 2 left, we show the model of a short shell ejection with mass loss corresponding to the peanut-shape. The corresponding image of AG Carinae (Nota & Clampin 1997) is shown in Fig. 2 right.

The anisotropies of mass loss influence the loss of angular momentum. Polar mass loss removes mass but relatively little angular momentum. This has a great incidence on the evolution of the most massive stars with high rotation (Maeder 2002). The mass loss rate  $\dot{M}(\Omega)$  of a rotating star compared to that  $\dot{M}(0)$  of a non-rotating star at the same location in the HR diagram is given by (Maeder & Meynet 2000),

$$\frac{\dot{M}(\Omega)}{\dot{M}(0)} \simeq \frac{(1 - \Gamma)^{\frac{1}{\alpha} - 1}}{\left[1 - \frac{4}{9} \left(\frac{v}{v_{\text{crit},1}}\right)^2 - \Gamma\right]^{\frac{1}{\alpha} - 1}}, \quad (2)$$

where  $\alpha$  is a force multiplier (Lamers et al. 1995). For a  $10 M_{\odot}$  star on the MS,  $\frac{\dot{M}(\Omega)}{M(0)}$  may reach 1.5. For the most luminous stars which have a value  $\Gamma$  close to 1.0, this may be orders of magnitude, when the star reaches break-up at the  $\Omega\Gamma$ -Limit.

Often, the critical velocity in a rotating star is written as  $v_{\text{crit}}^2 = \frac{GM}{R}(1 - \Gamma)$ . This expression is not correct, as it applies only to uniformly bright stars. Indeed, the critical velocity of a rotating star is given by the zero of the equation expressing the total gravity  $g_{\text{tot}} = g_{\text{grav}} + g_{\text{rot}} + g_{\text{rad}} = g_{\text{eff}} [1 - \Gamma_{\Omega}(\vartheta)]$ . This equation has two roots (Maeder & Meynet 2000). The first that is met determines the critical velocity. The first root is as usual  $v_{\text{crit},1} = \left(\frac{2}{3} \frac{GM}{R_{\text{pb}}}\right)^{\frac{1}{2}}$ , where  $R_{\text{pb}}$  is the polar radius at break-up. The second root  $v_{\text{crit},2}$  applies to Eddington factors bigger than 0.639. It is equal to 0.85, 0.69, 0.48, 0.35, 0.22, 0 times  $v_{\text{crit},1}$  for  $\Gamma = 0.70, 0.80, 0.90, 0.95, 0.98$  and 1.00 respectively.

### 3. Close to the Eddington Limit, evolution unavoidably reaches the $\Omega\Gamma$ -Limit

On the whole, we may distinguish 3 critical cases, where the outer layers escape: 1.- The usual  $\Gamma$ -Limit, when radiation effects largely dominate over rotation; this is the classical case. 2.- The  $\Omega$ -Limit, when rotation effects, rather than radiative effects, are determining break-up. This is relevant for Be-stars, which are far enough from  $\Gamma$  equal to unity. 3.- The  $\Omega\Gamma$ -Limit, when both rotation and radiation are important. This is the case which applies to the most massive stars. *Even for a rather small initial rotation velocity of, say,  $\geq 50$  km/s, a star with a high  $\Gamma$  will reach critical velocity during its MS evolution.* This occurs because the rotation velocity increases during MS evolution (see Fig. 3), while the critical velocity, which is given by  $v_{\text{crit},2}$ , decreases. The mass loss rates increase strongly (cf. Eq. 2), when the critical  $\Omega\Gamma$ -Limit is approached. Such a situation has already been considered (Langer 1997), however for the case of solid body rotation, while here the evolution of the angular momentum is followed with appropriate critical velocity and mass loss expressions.

The evolution of star reaching the  $\Omega\Gamma$ -Limit is illustrated in Fig. 3. On the left, it shows different cases of tracks in the HR diagram. The track with  $v_{\text{ini}} = 500$  km/s and an average mass loss rate  $\dot{M}$  of  $10^{-4.5} M_{\odot} \cdot \text{yr}^{-1}$  is calculated according to recent  $\dot{M}$ -rates (Vink et al. 2001). With these rates, even the zero rotation track would turn bluewards! Thus, at  $120M_{\odot}$ , these rates are likely too high (at least for producing a star like  $\eta$  Carinae). With rates a factor of 2-3 lower, a bluewards evolution is obtained only for a very fast rotation, such as 650 km/s. For initial rotation  $v_{\text{ini}} = 600$  km/s or lower, redward evolution is obtained, with tracks having a different MS extension (for low rotation, the tracks are higher and extend further in the HR diagram than the track for zero rotation; for fast rotation, the extension is shorter as the result of the lower opacity due to higher helium enrichment). All tracks with  $v_{\text{ini}} \geq 50$  km/s reach the  $\Omega\Gamma$ -Limit with break-up velocity, thus experiencing phases of extreme mass loss.

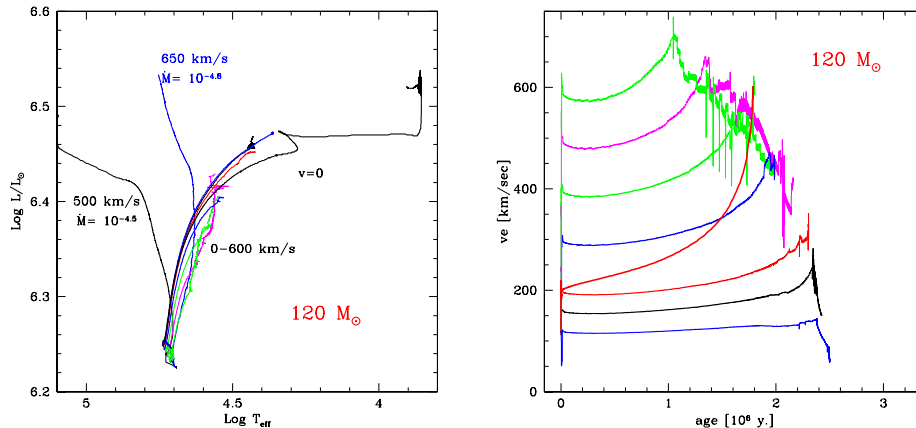


Figure 3. Left: Evolution of a  $120 M_{\odot}$  star with different mass loss rates and initial rotational velocities  $v_{\text{ini}}$ , see text. Right: Evolution of the rotational velocities of models with different  $v_{\text{ini}}$ . The envelope of the various curves is the location where the stars reach their critical velocities. The models with a lower  $v_{\text{ini}}$  reach the critical velocity later. A model with solid body rotation with  $v_{\text{ini}} = 200 \text{ km/s}$  is also shown. It reaches the critical velocity faster.

Fig. 3 right illustrates the corresponding behaviour of the rotational velocities. We see that the velocities increase during evolution. The faster  $v_{\text{ini}}$ , the earlier the  $\Omega\Gamma$ -Limit is reached (envelope of the curves). We see that solid body rotation, which is the extreme case of coupling of the angular momentum, leads the star very promptly to the  $\Omega\Gamma$ -Limit. The milder coupling realized by meridional circulation leads the star to the  $\Omega\Gamma$ -Limit more slowly. We conclude that the most massive stars reach an  $\Omega\Gamma$ -Limit, which is different for each star according to its rotational velocity. The  $\Omega\Gamma$ -Limit is the physical reason for the observed Humphreys–Davidson Limit (Humphreys & Davidson 1979).

#### 4. What occurs at the $\Omega\Gamma$ -Limit ?

For now, hydrodynamical models of LBV outbursts do not exist, nevertheless we can make a few remarks on their properties:

-1. Likely, the most massive stars reach the  $\Omega\Gamma$ -Limit on their redwards track as illustrated in Fig. 3 left. The slightly less massive stars, firstly evolving to the red, may likely reach the Limit on their bluewards tracks, because as a result of their mass loss, their  $L/M$  is larger when they go back to the blue. Also, due to the coupling of angular momentum by convection, they may rotate faster when evolving bluewards (Langer 1998).

-2. As stated above, the  $\dot{M}$ -rates increase as given by Eq. (2), when the  $\Omega\Gamma$ -Limit is approached. However, at the Limit, the  $\dot{M}$ -rates are no longer given by the stellar wind theory. We think that the  $\dot{M}$ -rates are such that the star just remains at the critical velocity, (or in practice, at a fraction e.g. 0.98 or 0.99 of it). If the  $\dot{M}$ -rates would be larger the star would soon become subcritical, if they would be smaller, the star would rotate much above critical.

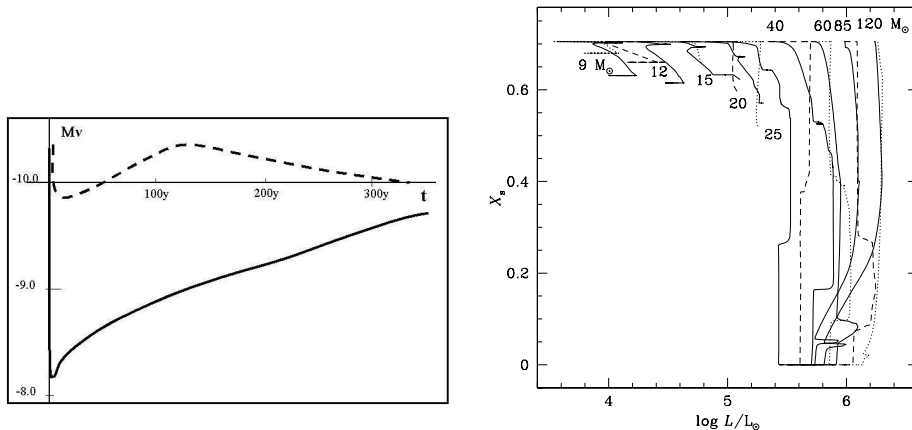


Figure 4. Left: The broken line shows the V–light curve for a star with  $\log T_{\text{eff}} = 3.8$  experiencing a mass ejection of  $1.0M_{\odot}$ , the continuous line shows the same for an ejection of  $3 M_{\odot}$ , the last part of this curve would be similar to the broken line. Right: Evolution of the massive stars in the plot of the surface H-content  $X_s$  vs. luminosity.

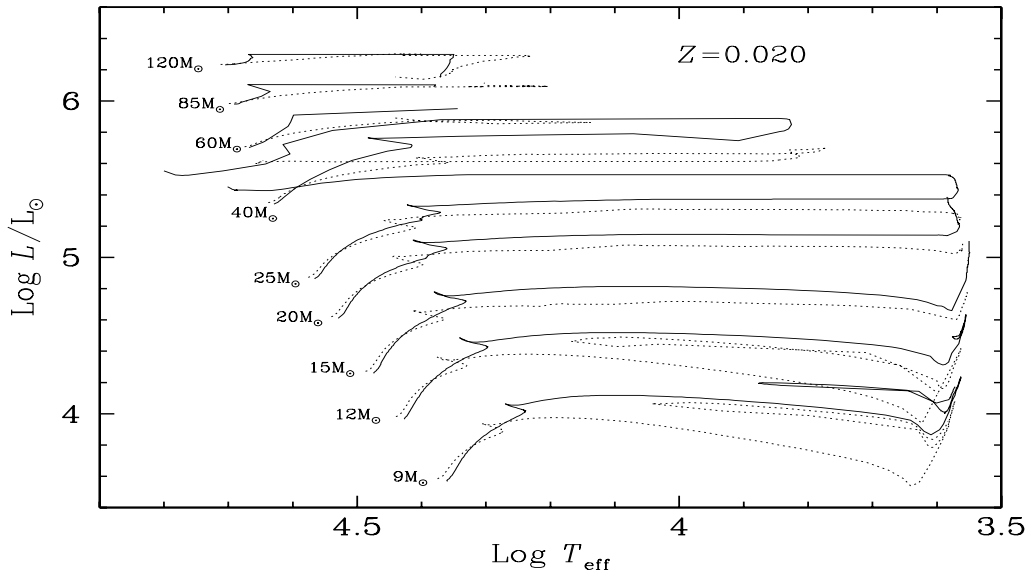
-3. Some layers become supra-Eddington, which produces a density inversion and convective instability appears. Thus, even a B–type supergiant can have convection in its outer layers (Maeder 1980).

-4. In the very massive stars, the thermal timescale may become smaller than the dynamical timescale in the outer layers. This means that the thermal structure of these layers can readjust during a dynamical event. Thus, the ionization front may move inwards and allow a substantial mass fraction to participate to a dynamical event. This is the idea of the “geyser model” (Maeder 1992; Humphreys & Davidson 1994; Maeder 1997), which leads to an estimate of the amount of mass ejected as a function of the luminosity. This has been confirmed by IRAS observations of dust in LBV nebulae (Hutsemekers 1997).

-5. As a result of the mass ejected in the outburst, the star is shifted to the blue in the HR diagram, then it slowly recovers its previous  $T_{\text{eff}}$ . The luminosity keeps nearly constant, apart from the energy lost in the mechanical event. Simulations of sudden large mass ejection show several properties: - a) The extension of blue shift in the HR diagram depends on the ejected mass  $\Delta M$ ; - b) The timescale of the blueshift is determined by the mass loss rate in the outburst; - c) The light curve in V magnitude (cf. Fig. 4 left) is mainly determined by the change of the bolometric correction (see lightcurve of  $\eta$  Car); - d) The recovery time, i.e. the time for the star to reach its former equilibrium depends on the ejected mass  $\Delta M$ . It is about 125, 350 and 750 yr for  $\Delta M = 0.3, 1.0$  and  $3.0 M_{\odot}$ .

## 5. Filiations and further evolution of the massive stars

There are various evolutionary sequences: for the highest masses with mass loss, the stars may keep to the blue. Then in an interval of lower masses, the tracks have a certain extension to the red and even in a lower mass interval the full


 Figure 5. HR diagram of massive stars with metallicity  $Z=0.02$ 

extension to the red supergiants is present (Fig. 5). We may distinguish the following tentative filiations at solar  $Z$ :

$M > 90 M_{\odot}$ : O - Of - WNL - (WNE) - WCL - WCE - SN (Hypernova low  $Z$ ?)

$60 - 90 M_{\odot}$ : O - Of/WNL < - > LBV - WNL (H poor) - WCL-E - SN(SNIIIn?)

$40 - 60 M_{\odot}$ : O - BSG - LBV < - > WNL - (WNE) - WCL-E - SN(SNIIb)  
- WCL-E - WO SN (SNIIc)

$30 - 40 M_{\odot}$ : O - BSG - RSG - WNE - WCE - SN(SNIIb)

OH/IR < - > LBV ?

$25 - 30 M_{\odot}$ : O - (BSG) - RSG - BSG (blue loop) - RSG - SN(SNIIb, SNIIc)

$10 - 25 M_{\odot}$ : O - RSG - (Cepheid loop,  $M < 15 M_{\odot}$ ) RSG - SN (SNIIc, SNIIp)

The sign < - > means back and forth motions between the two stages. The limits between the various scenarios depend on metallicity  $Z$  and rotation. The various types of supernovae are tentatively indicated.

The variation of the H-surface content  $X_s$  as a function of luminosity is a constraining test (Fig. 4). The most massive stars go almost vertically down. The LBV stars, according to a recent collection of data (Stothers & Chin 2000), are located between  $\log L/L_{\odot} = 5.4$  and  $6.2$  with  $X_s$  between  $0.30$  and  $0.40$ . The WN stars are in almost the same range of  $L$  while their  $X_s$  are between  $0.45$  and  $0$ . This overlap supports the back and forth transition between the WNL stars and the LBV. The further evolution from LBV leads them to WN stars, firstly WNL and then WNE. The WR lifetimes as a function of initial mass, rotation and  $Z$  have been calculated (Meynet & Maeder 2004). The comparison with observations is considerably improved when rotation is accounted for.

Fig. 6 left shows the relative enrichments in  $N/C$  for stars of  $9$  and  $40 M_{\odot}$  at different  $Z$ . In the lower mass domain, the enrichments are higher for stars with lower  $Z$  since mixing is in general stronger. This results from the steeper

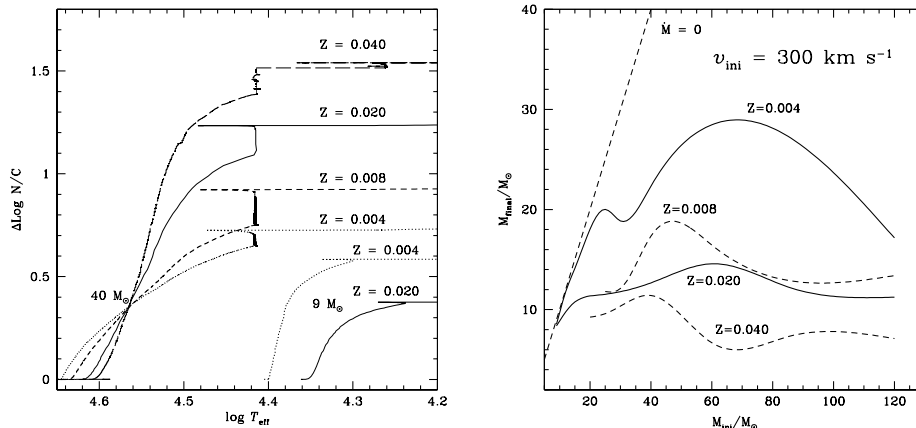


Figure 6. Left: Relative enrichments in N/C for rotating stars of 9 and  $40 M_{\odot}$  at different  $Z$  but with the same  $v_{\text{ini}} = 300 \text{ km/s}$ . Right: The final masses at the time of SN explosion as a function of mass and  $Z$ .

internal  $\Omega$ -gradients in lower  $Z$  stars (Meynet & Maeder 2001). For masses above  $30 M_{\odot}$ , mass loss dominates the evolution and as the  $\dot{M}$ -rates are larger at higher  $Z$ , the enrichments are also larger at higher  $Z$ .

## 6. Final stages in relation with $\gamma$ -ray bursts (GRBs)

As a result of mass loss, the stellar masses decrease very much. Fig. 6 right shows the final masses at the time of supernova explosion as a function of the initial masses and  $Z$ . For solar  $Z$  or higher, all stars with initial masses above  $20 M_{\odot}$  finish their life with masses of about  $10 M_{\odot}$ . At lower  $Z$ , the final masses are higher. It should not be concluded that for  $Z = 0$  the final masses are equal to the initial ones, because such stars are likely to spend a fraction of their MS lifetime at break-up and loose mass (see Meynet, this conference). The different final masses lead to different types of supernovae.

Fig. 7 left shows the distribution of the specific angular momentum  $j$  at various stages of an initial  $25 M_{\odot}$  star. The final distribution of  $j$  is essentially shaped during MS evolution. Thus, the treatment of the transport of angular momentum in the MS phase is an essential aspect. The various models (Heger et al. 2000; Heger et al. 2003; Hirschi et al. 2004) lead to rather similar distributions, despite their differences in input physics. A specific angular momentum above  $10^{16} \text{ cm}^2 \text{ s}^{-1}$  is necessary for the collapsar model to work (Heger et al. 2000; Heger et al. 2003) and account for the (GRB). These models fulfill this condition, however a lot of angular momentum has to be lost in the explosions in order to account for the rotation rate of pulsars.

The association of GRB with hypernovae of the class of SNIc is supported by several observations (Mazzali et al. 2003; Podsiadlowski et al. 2003). SNIc result from the explosion of a star without H and with little or no He. This corresponds to a rare category of WR stars: the so-called WO stars. WO stars are subsequent to WC3 objects, they show the products of He-burning,

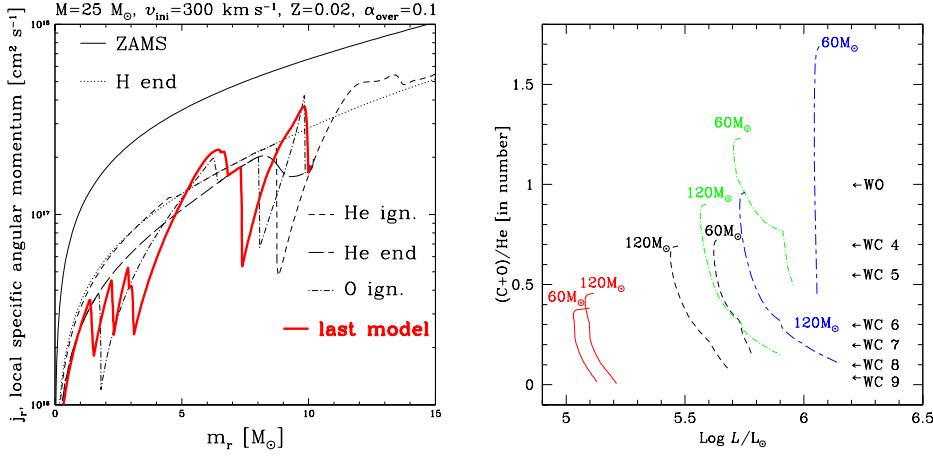


Figure 7. Left: Distribution of the specific angular momentum in a model with an initial mass of  $25 M_{\odot}$ . The distribution is shown at various evolutionary stages (Hirschi et al. 2004). The distribution in the last model coincide well with results from Heger et al. (Heger et al. 2000; Heger et al. 2003). Right: Evolution of the ratios  $(\text{C}+\text{O})/\text{He}$  as a function of the luminosity at the surface of 60 and 120  $M_{\odot}$  rotating models for various initial metallicities (see text). Long-short dashed curves, short-dashed curves and continuous lines show the evolutions for  $Z = 0.004$  models, dashed-dotted curves, short-dashed curves and continuous lines show the evolutions for  $Z = 0.008$ , 0.020 and 0.040 respectively. The correspondence between the  $(\text{C}+\text{O})/\text{He}$  ratios and the different WC subtypes (Smith & Maeder 1991) is indicated on the right.

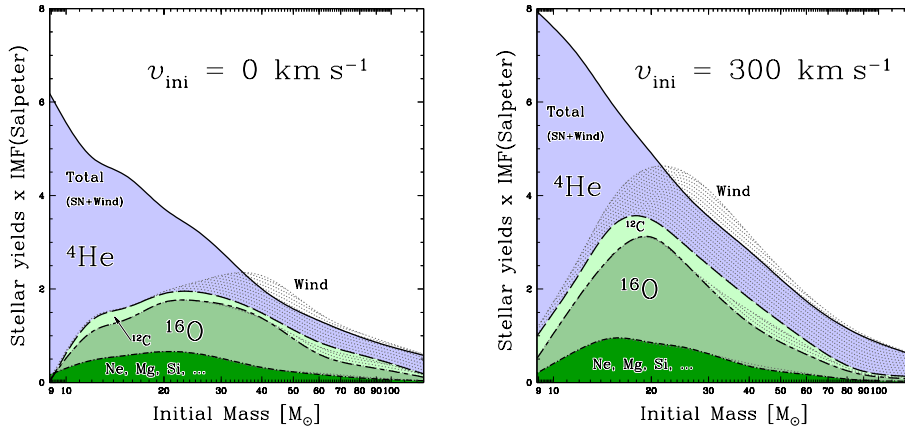


Figure 8. Left: the yields  $\times$  IMF for models without rotation. Right: the yields  $\times$  IMF for models with  $v_{\text{ini}} = 300 \text{ km/s}$  (Hirschi et al. 2004).

with an excess of C+O with respect to He and  $\text{O} > \text{C}$ . WO stars are rare and result from the evolution of stars with  $M \geq 60 M_{\odot}$  at low metallicity only (Smith & Maeder 1991). These authors show that early WC types and WO stars are found in lower  $Z$  regions. This may seem surprising. The reason is (Smith & Maeder 1991): at high  $Z$ , mass loss is high, thus when the products

of the  $3\alpha$  reaction appear at the surface, they are in an early stage of nuclear processing, i.e. with a low  $C + O/He$  ratio (see Fig. 7 right). This corresponds to late WC stars. At low  $Z$ , the products of the  $3\alpha$  reaction rarely appear at the stellar surface and if they do it (e.g. in case of high rotation) this occurs very late in the evolution, i.e. when  $C + O/He$  is high and this is a WO star (Smith & Maeder 1991). Thus, the rare WO stars may be the progenitors of SNIc and GRB.

Nucleosynthesis is also influenced by rotation (Hirschi et al. 2004). Below  $30 M_{\odot}$ , the  $\alpha$ -elements are enhanced due to the larger cores. Above  $30 M_{\odot}$ , mass loss is the dominant effect and more He is ejected before being further processed. Fig. 8 shows the yields multiplied by the initial mass function. Due to the weighting by the IMF, the production of oxygen and of  $\alpha$ -elements is globally enhanced, while the effect on the He-production in massive stars is rather small.

## References

- Heger, A., Langer, N. 1998, A&A 334, 210  
 Heger, A., Langer, N., & Woosley, S. E. 2000, ApJ, 528, 368  
 Heger, A., Woosley, S. E., Langer, N., & Spruit, H. C. 2003, astro-ph0301374  
 Herrero, A., Puls, J., Villamariz, M.R. 2000, A&A 354, 193  
 Hirschi, R., Meynet, G., Maeder, A. 2004, A&A, in press  
 Humphreys, R., Davidson, K. 1979, ApJ 232, 409  
 Humphreys, R., Davidson, K. 1994, PASP 106, 1025  
 Hutsemekers, D. 1997, in: Nota A., Lamers H. (eds.) Luminous Blue Variables: Massive Stars in Transition. ASP Conf. Series 120, p. 316  
 Lamers, H.J.G.L.M., Snow, T.P., Lindholm, D.M. 1995, ApJ 455, 269  
 Langer N., 1997, in: Nota A., Lamers H. (eds.) Luminous Blue Variables: Massive Stars in Transition. ASP Conf. Series 120, p. 83  
 Langer N., 1998, A&A 329, 551  
 Maeder, A. 1980, A&A 90,311  
 Maeder, A. 1992, Proc. of the Int. Conf. Amsterdam, Ed. C. de Jager & H. Nieuwenhuijzen, North Holland, p.138.  
 Maeder, A. 1997, in: Nota A., Lamers H. (eds.) Luminous Blue Variables: Massive Stars in Transition. ASP Conf. Series 120, p. 374  
 Maeder, A. 1999, A&A 347, 185 (paper IV)  
 Maeder, A. 2002, A&A 392, 575 (paper IX)  
 Maeder, A., Desjacques, V. 2000, A&A 372, L9  
 Maeder A., Meynet G. 2000, A&A 361, 159 (paper VI)  
 Maeder A., Meynet G. 2001, A&A 373, 555 (paper VII)  
 Mazzali, P.A., Iwamoto, K., Nomoto, K. 2003, ApJ 599, L95  
 Meynet G., Maeder A. 1997, A&A, 321, 465 (Paper I)  
 Meynet G., Maeder A. 2004, A&A, in press(Paper XI)  
 Nota A., Clampin M. 1997, in *Luminous Blue Variables: massive stars in transition*, Eds. A. Nota & H.J.G.L.M. Lamers, ASP Conf. Ser. 120, p. 303  
 Podsiadlowski, Ph., Mazzali, P.A., Iwamoto, K., Nomoto, K., Lazzati, D., Cappellaro, E. 2003, ApJ 607, L17  
 Smith, L.F., Maeder, A. 1991, A&A, 241, 77  
 Stothers, R., Chin, C.W. 2000, ApJ 540, 1041  
 Vink, J.S., de Koter, A. & Lamers, H.J.G.L.M. 2001, A& A 362, 295  
 Zahn J.P. 1992, A&A 265, 115